Microstructuring of Graphene Oxide Nanosheets Using Direct Laser Writing

By *Yong Zhou, Qiaoliang Bao, Binni Varghese, Lena Ai Ling Tang, Chow Khim Tan, Chorng-Haur Sow,* and *Kian Ping Loh**

Graphene (G), a single atomic layer of aromatic carbon atoms, has attracted much attention recently owing to its fascinating properties such as massless fermions, ballistic electronic transport, and ultrahigh electron mobility.[1] Currently, there are many approaches to the synthesis of graphene ranging from chemical vapor deposition from hydrocarbon to solution phase methods involving the chemical exfoliation of graphite.[2] One commonly used solution-processing route to graphene involved the chemical reduction of graphene oxide (GO). GO is produced by the oxidative treatment of graphite.[2] The basal planes of GO are decorated with epoxide and hydroxyl groups, while carboxylic and carbonyl groups are located at the edges. These oxygen functionalities render GO hydrophilic and improve its solubility, however they destroy the aromaticity of the graphene framework. As a result, GO is insulating, and a chemical reduction and thermal annealing treatment is needed before electronic conductivity could be recovered. The presence of oxygen functional groups also reduces the thermal stability of GO relative to that of G, since GO can be thermally pyrolized at high temperatures and transformed into volatile carbonaceous oxides. The thermal instability of GO motivates us to consider a strategy for the microstructuing of GO nanosheets using laser-assisted etching. The microstructuring of GO is relevant to the challenges of lithographically patterning G, since GO and G are interconvertible to some extent. Recently, promising approaches for the patterned assemblies of G on substrates have been developed.[3–8] Micro-contact printing using molecular templates was used to transfer GO sheets onto the pre-defined areas of the substrate surfaces via electrostatic attachment.[3] Large-scale G films were recently synthesized on patterned nickel layers using chemical vapor deposition.[7] All the patterning methods reported so far involved conventional lithographic techniques or employment of masks for the definition of patterns on substrates. To date, there are few demonstrations of a maskless, direct ''writing'' pattern on G-related materials using electron beam or optical methods.

[*] Prof. K. P. Loh, Dr. Y. Zhou, Dr. Q. Bao, L. A. L. Tang, C. K. Tan
Department of Chemistry, Faculty of Science, National University of Singapore (NUS)
3 Science Drive 3, 117543 (Singapore)
E-mail: chmlohkp@nus.edu.sg
Dr. B. Varghese, Prof. C.-H. Sow
Department of Physics, Faculty of Science, National University of Singapore (NUS)
Singapore 117542 (Singapore)

DOI: 10.1002/adma.200901942

Focused laser beam has been an important research tool in the surface modification or microstructuring of thin films.[9] The essence of this technique is the creation of an effective heat zone by the focused laser beam which induces a localized physical state transition. With sufficient laser power, ablation of materials such as steel, ceramics,[10,11] nanostructures,[12] and biological samples like human tooth can occur.[13]

In this Communication, we employed a focused laser beam technique to construct an extended area of micropatterned GO and reduced GO multilayers on quartz substrates in a fast and controlled manner. The advantage of this technique is its reliability, amenability, upwards scalability and low cost. Most importantly, the creation of patterned features does not require the use of any pre-defined patterned substrates.

Electrostatic layer-by-layer (LBL) assembly techniques were employed to grow multilayers of GO film on a quartz substrate with polyethylenimine (PEI) as a linker (Process 1, abbreviated as P1).[14] At the single layer stage, atomic force microscope (AFM) imaging of the film displays continuous monolayer film of assembled GO (see Fig. S1a and b in Supporting Information). The height profile reveals the thickness of the GO nanosheet to be 1.5 nm. The consecutive buildup of the LBL PEI/GO film was monitored by UV-vis absorption spectroscopy (Fig. S1c). The pronounced peak at 227 nm can be assigned to $\pi \rightarrow \pi^*$ transitions of aromatic C=C bonds. The linear increase in absorbance as a function of the number of layers deposited (inset of Fig. S1c) indicates very uniform increase of layer thickness in each dipping cycle.

The setup of the optical microscope-focused laser beam system used in this work was described in our previous work.[12] The laser used in this work is a continuous wave diode laser with wavelength of 663 nm and a maximum output power of 80 mW. The laser beam diameter is around 3 μm. Figure 1 schematically illustrates the procedures of patterning GO and the conversion to reduced GO multilayer films. The film was placed in the focused laser-beam system. When the focused laser beam was incident on the multilayer GO film, the irradiated area absorbed the laser energy, and the energy was rapidly converted into local heat. The intense heating raised the temperature of the irradiated area above 500 °C in air and resulted in localized oxidative burning of GO to volatile gases such as CO or CO_2 (Fig. 1-P2 and P3). By moving the computer-controlled sample stage in a programmable step with respect to the focused laser beam, patterns with tunable width and length could be directly written. Examples include periodic micro-channels and square pillar as reported in the present work (Fig. 1-P4 and P5). The patterned GO can be subsequently reduced to G by exposure to hydrazine gas or

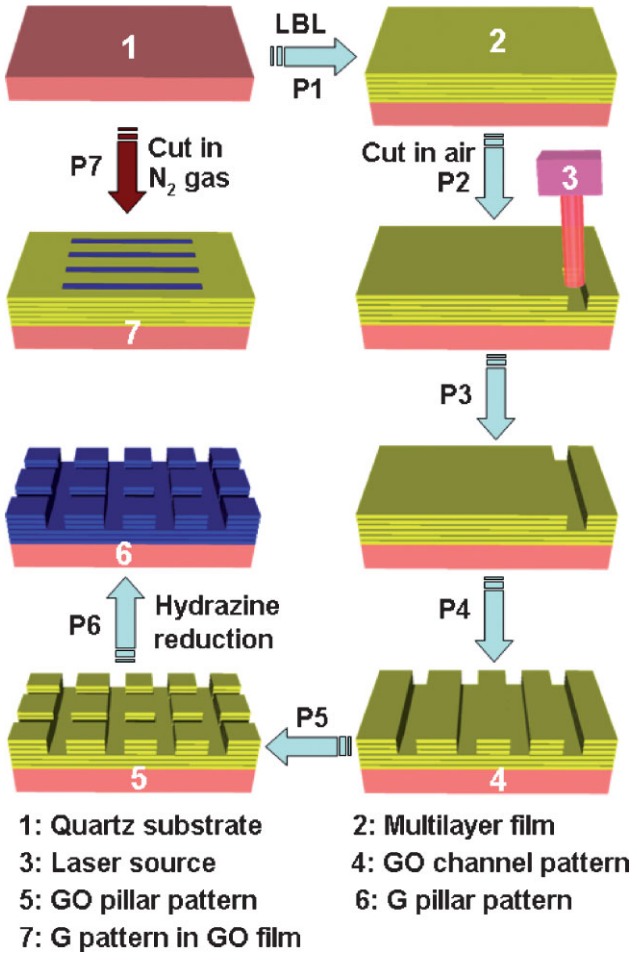

Figure 1. Schematic illustration of the creation of microfeatures on GO nanosheets with an optical microscope-focused laser beam.

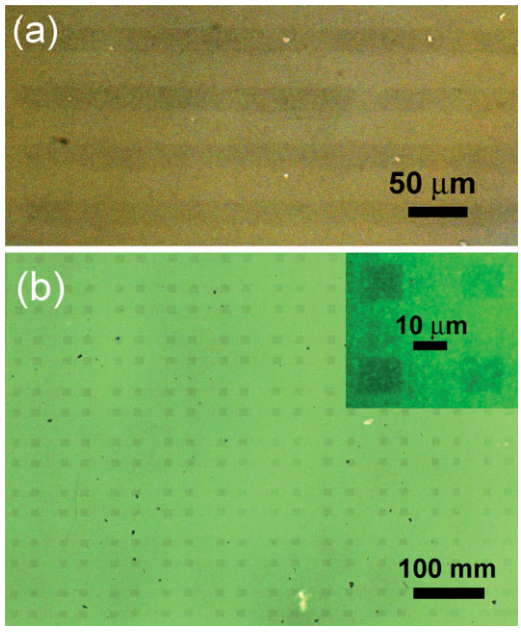

Figure 2. Optical microscope images of a) the channel and b) the square patterns created by laser-cutting of the 6-layer film. The bright region corresponds to cut area, and dark region to the uncut one. Inset of (b) is the magnified image.

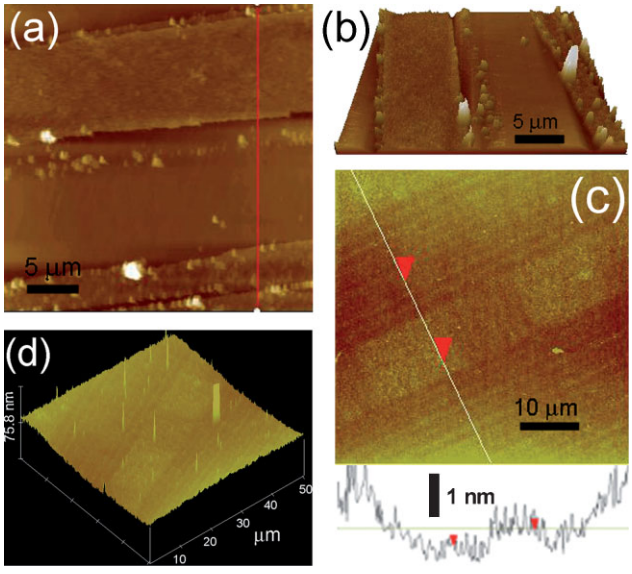

Figure 3. a) 2D and b) 3D AFM images of the channel pattern, c) 2D AFM image of the square pillar and the corresponding height profile, and d) 3D AFM image of the square pillar.

thermal annealing at high temperatures (Fig. 1-P6). The above procedures described the laser cutting in air where oxidative burning of the localized heated area occurs. When the focused laser-beam cutting of the GO film was carried out with the sample housed in an inert environment (N_2 gas), we found that oxidative burning did not occur and no cutting was obtained. Instead, the GO was deoxygenated or thermally reduced to G in this case. In other words, the direct writing of conductive G pattern on GO films, where the G domains were isolated by insulating GO matrix, was achieved (Fig. 1-P7). This presents very unique advantages in device fabrication, which cannot be achieved by any other techniques so far.

The optical microscopy images demonstrate the formation of periodic arrays of GO channel (Fig. 2a) and square pillar (Fig. 2b) via the laser-cutting of the 6-layer GO film. The bright and the dark colored areas correspond to the cut and uncut regions, respectively. The difference in color of the patterned film is due to optical contrast arising from different thickness of the GO.[15] The width of channel and the side length of the square pillar are approximately 20 μm, respectively. The AFM images display the 2D and 3D views of the channel (Fig. 3a and b) and square pillar (Fig. 3c and d) patterns. The precipitates observed in Figure 3a originate from impurities due to incompletely exfoliated graphite, which cannot be removed by laser irradiation. The cut trace can be clearly seen in Figure 3c. The height profile demonstrates the height of the pillar to be about 4.5 nm, corresponding to the thickness of 3-layer GO. It indicates that the laser beam did not remove the entire layers of the GO film, but 3 layers remained. Hence by scanning the laser beam back and forth across the film

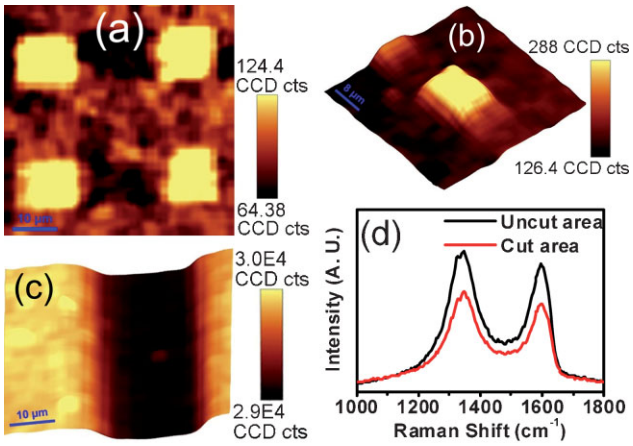

Figure 4. a) 2D and b) 3D Raman mapped images of the square pillar pattern of the GO. c) 3D Raman mapped image of the channel pattern. All the Raman images are generated from the intensity of G band. d) Raman spectra of the cut and uncut area.

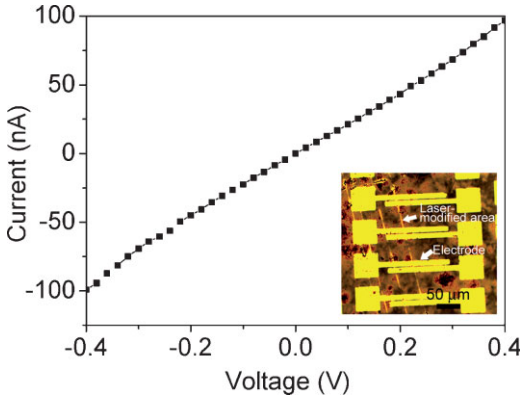

Figure 5. *I–V* curve of laser-modified area irradiated in N_2 gas. Inset: representative optical microscope image of the electrodes on the modified area.

with small advancing step, we can fabricate periodic channels with tunable width (Fig. S2).

The thickness of the laser-cut GO films, as well as the occurrence of any phase changes following the laser treatment, was tracked using spatially resolved Raman imaging. Raman mapping of the square pillar configuration and the channel are shown in Figure 4a–c, respectively. Raman spectroscopy performed on the patterned domains shows that both cut and uncut regions display the D and G bands at 1348 cm^{-1} and 1566 cm^{-1}, respectively (Fig. 4d). A reduction by half of the D and G band intensities was observed on the cut region compared to uncut region, which indicates that loss of carbon material occurred during the laser treatment. We find that there is a linear relationship between the intensity of the Raman band and the number of the GO layers (Fig. S3). The linear relation allows us to deduce that the laser irradiation removed only the upper 3 layers of the 6-layer GO, and the bottom 3 layers remained. The position and shape of the Raman peaks before and after laser treatment are very similar, and no broadening of the peak attributed to amorphous carbon is observed.[16] This suggests the GO was removed cleanly and not transformed into amorphous carbon.

The amount of laser energy absorbed is proportional to the adsorption coefficient as well as the amount of the adsorbing materials. We observed that the laser cutting worked only for GO films with layered thickness exceeding 6 layers. For instance, a 10-layer film could be cut successfully (Fig. S4), although the increasing roughness of the film surface with the increasing number of layers makes it difficult to accurately determine the thickness of cut GO. For GO films that are thinner than 6 layers, the GO film remain intact even after prolonged laser irradiation within the limits of the laser power in our experiments. It is found that films of 1−4 layers cannot be cut at all (Fig. S5a) and the cutting process has poor reproducibility on the 5-layer film (Fig. S5b) using the same cutting procedure.

As expected of a thermally induced cutting process, we find that the thermal conductivity of the substrate plays a critical role on the successful patterning of the GO film with the present laser technique. When the 6-layer GO film is assembled on a silicon substrate, no cut trace can be observed with the same laser cutting procedure. This could be explained by the much higher thermal conductivity (~148 W m^{-1} K^{-1} at 1 atm and 25 °C)[17] of silicon compared to quartz glass (~1.5 W m^{-1} K^{-1} at 1 atm and 25 °C). The laser energy absorbed by the film can be easily transferred to the substrate, which was subsequently quickly dissipated.

The patterned GO film can be chemically reduced to G upon exposure to hydrazine vapor at 80 °C for 6 h, in accordance with similar chemical reduction process reported before.[18] We discovered that reduction to G could also be attained by the laser modification of the GO film in an inert atmosphere (N_2), which prevents oxidative burning. Raman analysis did not detect any significant changes in the intensity of the Raman bands between the cut and uncut regions, implicating no significant mass loss detectable by Raman spectroscopy. To measure the changes in conductivity of the film before and after laser treatment, electrodes were deposited on the GO film. The electrical measurement showed that the laser-modified region displayed appreciable conductivity of ~1.1 S m^{-1} compared to the totally insulating GO before laser irradiation (Fig. 5). This is indicative of a reduction of GO into G, arising possibly from thermal induced desorption of the surface oxygen groups and reconstruction of the surface.[19] Therefore, the laser writing may constitute as a powerful approach for the direct-writing of graphene channels isolated by GO dielectric.

One question remained. Why was a 6-layer GO film cut to 3-layer film, and no further? A theoretical simulation was carried out to provide an insight into the heat adsorption and subsequent cutting performance during laser irradiation on the GO film. The dynamics of laser heating can be considered as a typical 3D heat flow problem, which can be simulated by the solution of the heat conduction equations. The energy losses due to radiation and convection to the ambient are negligible with respect to the energy absorbed in the considered GO films. Thus, the surface of GO thin films can be assumed to be adiabatic. The differential equation for heat conduction can be written in terms of the

temperature distribution $T(x,y,z,t)$ at varied position and time t as[20]

$$\rho C_P \frac{\partial T(x,y,z,t)}{\partial t} = \frac{\partial}{\partial x}(\kappa \frac{\partial T(x,t)}{\partial x}) + \frac{\partial}{\partial x}(\kappa \frac{\partial T(y,t)}{\partial y}) + \frac{\partial}{\partial x}(\kappa \frac{\partial T(z,t)}{\partial z}) + \alpha I(x,y,z) \quad (1)$$

where ρ is the mass density, C_p is the specific heat, α is the absorption coefficient, and κ is the thermal conductivity. The laser power density $I(x, y, z)$ is determined by the interaction of the laser radiation with the GO film and the subsequent transfer of the energy to the lattice. The laser power absorbed by each layer can be considered to have an exponential decay and written as:

$$I(x,y,z) = (1-R)I_0(x,y)\exp(-az) \quad (2)$$

where R is the reflectivity and $I_0(x, y)$ is the temporal distribution of the laser power. The laser source irradiation has the Gaussian profile:[12]

$$I_0(x,y) = I_0 \exp\left[-\left(\frac{x^2+y^2}{r_g^2}\right)\right] \quad (3)$$

where r_g is the radius of the Gaussian laser beam and I_0 is the inward heat flux (3.4×10^9 W m^{-2}).

We employed the finite element method (FEM) to compute the time-dependent temperature of GO layers under laser scanning (see Supporting Information, Fig S6). The thermal conductivity and specific heat capacity of GO was assumed to be similar to amorphous carbon in this calculation (refer Table 1 and 2 in Supporting Information). Figure 6 shows the simulated temperature fields in top surface of the GO thin films with different layers under laser irradiation. The calculation shows that the laser irradiation elevates the surface temperature of the GO film to a nearly constant value within 0.01 second, and this is enhanced with the increasing thickness of the GO layers due to increasing absorption. While the highest temperatures attainable for the uppermost layers of the GO films containing fewer than 5 layers are below 400 °C, the uppermost layers of the 6-layer GO film can reach temperature above 500 °C, as indicated by the red circled area with diameter of about 500 nm. As the desorption of oxygen functional groups of GO was reported at around 200–230 °C, and the oxidation of the carbon backbone is anticipated above 500 °C,[21] the numerically calculated temperature fields clearly reveal that: (1) GO films consisting of more than 6 layers can be burned off under laser shinning; (2) 5-layer GO can only be partially removed; (3) thin films with less than 5 layers GO cannot be burned off due to insufficient adsorption of thermal energy, although the laser heating might induce removal of functional groups. The simulation results are consistent with our experimental observation.

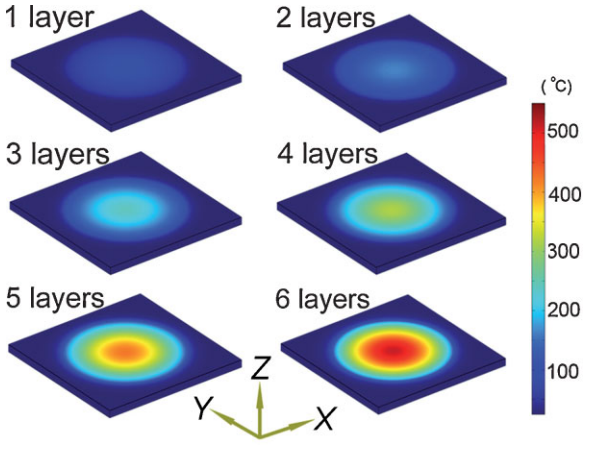

Figure 6. Temperature fields in top surface of GO thin films with varied number of layers. The temperature fields are captured at 0.01 s under laser shinning.

The temperature gradient inside the 6-layer GO thin film was calculated. The calculation shows that the temperature decreases along the depth and falls by ~100 °C from the top layer to the bottom layer (Fig. S7). The layer-by-layer stacked GO can be expected to have a larger in plane thermal conductivity compared to the out of plane, hence heat conduction in the vertical direction will be less efficient. The temperature of the upper 3 layers can reach ~500 °C while the temperature of the bottom 3 layers is significantly below 500 °C. This indicates that the upper 3 layers of GO can be burnt off under laser illumination, while the bottom layers remain. The remaining three layers do not have sufficient thermal energy to be burnt off and hence become thermally stable. This explains the incomplete removal of GO thin films (>6 layers) in our experiments and also reveals the surprising results that thin GO films can be more stable than thick films with regard to thermal damage threshold.

There are several salient features regarding the conditions needed for successful laser etching on GO that must be pointed out. First, we observed that the laser etching did not work on reduced GO that has been chemically reduced and annealed. The reduced GO sheets appear to be thermally stable in air, due perhaps to the recovery of the aromatic structures following the loss of oxygen groups. Second, the laser etching did not work in inert atmosphere. It is known that the interlayer distance in GO is affected by the humidity, due to the intercalation by water molecules.[2] One possibility is the instantaneous generation of steam from these intercalated water during laser irradiation expands the GO sheets and favors its exfoliation and decomposition in air.

In conclusion, we have implemented an inherently parallel and high throughput technique for creating "direct-write" features on GO samples. The laser cutting arises from the oxidative burning of the GO films in air. Thick films (>5 layers) can adsorb sufficient thermal energy to reach the evaporation temperature needed for forming oxidized carbonaceous materials, as opposed to thin films (<5 layers). As a result, the laser etching is self-terminating and a 6-layer film is uniformly cut to a 3-layer film. In view of the recent discovery that trilayer graphene is a semimetal with electrical behavior markedly different from single or bilayer G,[22] the ability to self-terminate the cutting to a 3-layer GO film affords a route to trilayer G films from thick films of non-uniform thickness. In addition, in inert atmosphere, the

laser causes a reduction of the GO to G, so this method provides a method to create G channels within the matrix of insulating GO. It can be anticipated that by optimizing parameters like the thermal conduction properties and temperature of the substrate as well as the energy of the laser, a greater degree of control in terms of trimming the layers to the desired thickness may be possible.

Experimental

Preparation of GO: GO was prepared using a modified Hummers' method from graphite powders (Grade 230 U kindly presented by Asbury Graphite Mills Inc. Kittunning, Pa) [23].

LBL Assembled GO Multilayer Film: A surface-cleaned quartz glass substrate was modified by treatment with a protonic PEI aqueous solution of 2.5 g dm^{-3} at pH 9.0 for 20 min to introduce positive charge to the substrate surface, followed by thorough washing with water and drying under N_2 flow. The protonic-PEI treated substrate was then immersed in negatively charged GO nanosheets solution at pH 9.0 for 20 min, followed by rinsing with water and drying under N_2 flow. By repeating the above steps, the desired number of GO layers can be achieved.

Laser Cutting: The optical microscope-focused laser beam setup was described in our previous work [12]. The laser beam was focused with a 50 × objective lens with a working distance of 8.3 mm. The laser used was a continuous wave diode laser with wavelength of 663 nm and a maximum output power of 80 mW. The laser beam was directed towards the objective lens of the microscope via a beam splitter and was focused tightly onto the GO multilayer film. The power of the laser beam after passing through the system of lens and mirrors was reduced to ~30% of the original emitted power. The scan rate of the laser beam on substrate is 15 μm s^{-1} and the laser beam diameter is around 3 μm. The laser power density irradiated on sample surface is 3.4×10^9 W m^{-2}. The sample was mounted on a computer controlled *x*–*y* motorized stage such that during the process of laser patterning the film was moved relative to the focused laser beam.

Characterization: The optical microscopy images were taken on Carl Zeiss with AxioCam MRc5. AFM images were taken with Dimension 3100, Digital Instruments, Veeco Metrology Group. The UV-vis absorption spectra were recorded on a Shimadzu UV 2450PC spectrophotometer. Field Emission Scanning Electron Microscope (FE-SEM) images were obtained with a FE scanning electron microanalyzer (JEOL-6300F, 5 kV). The Raman spectra were obtained with a WITEC CRM200 Raman system [24]. The excitation source is a 532 nm laser (2.33 eV) with a laser power below 0.1 mW on the sample to avoid laser-induced local heating. A 100 × objective lens with a numerical aperture (NA) of 0.95 was used in the Raman experiments, and the spot size of a 532 nm laser was estimated to be 500 nm. The spectra resolution of our Raman system is 1 cm^{-1}.

Acknowledgements

Y. Zhou and Q. L. Bao contributed equally to the project. The authors wish to acknowledge the support of the NRF-CRP grant "Graphene Related Materials and Devices R-143-000-360-281" for the support of this project. Supporting Information is available online from Wiley InterScience or from the author.

Received: June 9, 2009
Revised: June 27, 2009
Published online:

[1] a) F. Wang, Y. Zhang, C. Tian, C. Girit, A. Zettl, M. Crommie, Y. R. Shen, *Science* **2008**, *320*, 206. b) K. S. Novoselov, A. K. Geim, S. V. Morozov, D. Jiang, M. I. Katsnelson, I. V. Grigorieva, S. V. Dubonos, A. A. Firsov, *Nature* **2005**, *438*, 197. c) Y. Zhang, Y. W. Tan, H. L. Stormer, P. Kim, *Nature* **2005**, *438*, 201. d) A. K. Geim, K. S. Novoselov, *Nat. Mater.* **2007**, *6*, 183. f) S. V. Morozov, K. S. Novoselov, M. I. Katsnelson, F. Schedin, L. A. Ponomarenko, D. Jiang, A. K. Geim, *Phys. Rev. Lett.* **2006**, *97*, 016801/1.

[2] S. Park, R. S. Ruoff, *Nat. Nanotechnol.* **2009**, *4*, 217.

[3] Z. Wei, D. E. Barlow, P. E. Sheehan, *Nano Lett.* **2008**, *8*, 3141.

[4] X. Liang, Z. Fu, S. Y. Chou, *Nano Lett.* **2007**, *7*, 3840.

[5] C. Di, D. Wei, G. Yu, Y. Liu, Y. Guo, D. Zhu, *Adv. Mater.* **2008**, *20*, 3289.

[6] T. R. Hendricks, J. Lu, L. T. Drzal, I. Lee, *Adv. Mater.* **2008**, *20*, 2008.

[7] K. S. Kim, Y. Zhao, H. Jang, S. Y. Lee, J. M. Kim, K. S. Kim, J. H. Ahn, P. Kim, J. Y. Choi, B. H. Hong, *Nature* **2009**, *457*, 706.

[8] a) A. Turchanin, A. Beyer, C. T. Nottbohm, X. Zhang, R. Stosch, A. Sologubenko, J. Mayer, P. Hinze, T. Weimann, A. Gölzhäuser, *Adv. Mater.* **2009**, *21*, 1233. b) M. J. Allen, V. C. Tung, L. Gomez, Z. Xu, L. Chen, K. S. Nelson, C. Zhou, R. B. Kaner, Y. Yang, *Adv. Mater.* **2009**, *21*, 2098. c) L. Song, L. Ci, W. Gao, P. M. Ajayan, *ACS Nano* **2009**, *3*, 1353. d) S. Pang, H. N. Tsao, X. Feng, K. Müllen, *Adv. Mater.* **2009**, DOI: 10.1002/adma.200803812. e) G. Eda, G. Fanchini, M. Chhowalla, *Nat. Nanotechnol.* **2008**, *3*, 270.

[9] D. Bauerle, *Laser Processing and Chemistry*, 3rd ed. Springer, Berlin **2000**.

[10] G. F. Chen, X. F. Xu, C. C. Poon, A. C. Tam, *Opt. Eng.* **1998**, *37*, 2837.

[11] W. W. Duley, *UV Lasers: Effects and Applications in Material Science*, Cambridge University Press, New York **1996**.

[12] K. Y. Lim, C. H. Sow, J. Y. Lin, F. C. Cheong, Z. X. Shen, J. T. L. Thong, *Adv. Mater.* **2003**, *15*, 300.

[13] S. R. Franklin, P. Chauhan, A. Mitra, R. K. Thareja, *J. Appl. Phys.* **2005**, *97*, 094919.

[14] a) N. A. Kotov, I. Dekany, J. H. Fendler, *Adv. Mater.* **1996**, *8*, 637. b) D. Li, M. B. Muller, S. Gilje, R. B. Kaner, G. G. Wallace, *Nat. Nanotechnol.* **2007**, *3*, 101.

[15] P. Blake, E. W. Hill, A. H. Castro Neto, K. S. Novoselov, D. Jiang, R. Yang, T. J. Booth, A. K. Geim, *Appl. Phys. Lett.* **2007**, *91*, 063124.

[16] E. Cappelli, C. Scilletta, S. Orlando, V. Valentini, M. Servidori, *Appl. Surf. Sci.* **2009**, *255*, 5620.

[17] H. R. Shanks, P. D. Maycock, P. H. Sidles, G. C. Danielson, *Phys. Rev.* **1963**, *130*, 1743.

[18] a) H. A. Becerril, J. Mao, Z. Liu, R. M. Stoltenberg, Z. Bao, Y. Chen, *ACS Nano* **2008**, *2*, 463. b) S. Wang, P. J. Chia, L. L. Chua, L. H. Zhao, R. Q. Png, S. Sivaramakrishnan, M. Zhou, R. G. S. Goh, R. H. Friend, A. T. S. Wee, P. K. H. Ho, *Adv. Mater.* **2008**, *20*, 3440.

[19] Y. Zhou, Q. L. Bao, L. Tang, Y. L. Zhong, K. P. Loh, *Chem. Mater.* **2009**, *21*, 2950.

[20] a) T. Nakamiya, S. Aoqui, K. Ebihara, *Diamond Relat. Mater.* **2001**, *10*, 905. b) T. Nakamiya, T. Ueda, T. Ikegami, K. Ebihara, R. Tsuda, *Curr. Appl. Phys.* **2008**, *8*, 400.

[21] a) Z. H. Liu, Z. M. Wang, X. Yang, K. Ooi, *Langmuir* **2002**, *18*, 4926. b) R. Bissessur, P. K. Y. Liu, W. White, S. F. Scully, *Langmuir* **2006**, *22*, 1729. c) H. K. Jeong, M. H. Jin, K. P. So, S. C. Lim, Y. H. Lee, *J. Phys. D* **2009**, *42*, 065418. d) H. K. Jeong, Y. P. Lee, M. H. Jin, E. S. Kim, J. J. Bae, Y. H. Lee, *Chem. Phys. Lett.* **2009**, *470*, 255.

[22] M. F. Craciun, S. Russo, M. Yamamoto, J. B. Oostiya, A. F. Morpunzo, S. Tamura, *Nat. Nanotechnol.* **2009**, *4*, 383.

[23] J. C. Laura, K. Franklin, J. Huang, *J. Am. Chem. Soc.* **2009**, *131*, 1043.

[24] a) Z. Ni, Y. Wang, T. Yu, Y. You, Z. Shen, *Phys. Rev. B* **2008**, *77*, 235403. b) Z. Ni, H. Z. Wang, J. Kasim, H. M. Fan, T. Yu, Y. H. Wu, Y. P. Feng, Z. X. Shen, *Nano Lett.* **2007**, *7*, 2758.